SUPPORTING INFORMATION

Kinetic Models of Cyclosporin A in Polar and Apolar Environment Reveal Multiple Congruent Conformational States

Jagna Witek,[†] Bettina G. Keller,[‡] Markus Blatter,[¶] Axel Meissner,[¶] Trixie Wagner,[¶] and Sereina Riniker[*,†]

†*Laboratory of Physical Chemistry, ETH Zürich, Vladimir-Prelog-Weg 2, 8093 Zürich, Switzerland*

‡*Department of Biology, Chemistry, Pharmacy, Freie Universität Berlin, Takustrasse 3, 14195 Berlin, Germany*

¶*Novartis Institutes for BioMedical Research, Novartis Pharma AG, Novartis Campus, 4002 Basel, Switzerland*

E-mail: sriniker@ethz.ch

NMR measurements

Sample preparation

3.5 mg of lyophilized cyclosporine A (CsA) were dissolved in 40 μl de-acidified $CDCl_3$, vortexed for 20 s and transferred into 1.7 mm SampleJet NMR sample tubes. Samples were spun down into the tube using a Hettich manual centrifuge. Tubes were then closed by pressing a POM ball into the funnel of the tube cap. Tubes were then inserted into 1.7 mm

shuttles and placed on the automatic sample changer.

Data acquisition and processing

^1H detected 1D and 2D NMR spectra were obtained using a Bruker 600 MHz AVANCE III spectrometer equipped with a 1.7 mm TCI cryo probe and a z-gradient system. 1D proton spectra were recorded with a standard one-pulse sequence (30 degree flip angle) with a relaxation delay of 1 s and an acquisition time of 2.73 s. 16 scans of 65536 points covering 12019.23 Hz were recorded. For determination of amide temperature coefficients data was recorded in a range of 275 to 300 K. Data was zero-filled to 65536 complex points and an exponential window function was applied with a line-broadening factor of 0.3 Hz prior to Fourier transformation.

All 2D experiments for NMR assignment were recorded at a temperature of 300K with a relaxation delay of 1.5 s. For gradient COSY spectra[1,2] a data matrix of 512 x 2048 points covering 6602.1 x 6602.1 Hz was recorded with 1 scans for each increment. Data was linear predicted to 1024 x 2048 points using 32 coefficients and zero filled to 2048 x 2048 points. A sine square bell shaped window function was applied in F2 and a cosine square bell shaped window function in F1, respectively, prior to magnitude mode type 2D Fourier transformation. For edited coherence order selective gradient HSQC spectra[3,4] using adiabatic inversion pulses on the carbon channel,[5] a data matrix of 256 x 2048 points covering 24901 x 8417.5 Hz was recorded using 2 scans for each increment. Data was linear predicted to 512 x 2048 points using 32 coefficients and zero filled to 1024 x 2048 points prior to echo-anti echo type 2D Fourier transformation. A sine square bell shaped window function shifted by $\pi/2$ in both dimensions was applied. For HMBC spectra,[6] a data matrix of 320 x 4096 points covering 33805 x 8417.5 Hz with 8 scans for each increment was recorded using a double low pass J-filter and F1 absorption mode.[7] Data was linear predicted to 640 x 4096 points using 32 coefficients and zero-filled to 1024 x 2048 complex points prior to echo-anti echo type 2D Fourier transformation. A cosine square shaped window function was applied in

F1 and a sine shaped window function shifted by $\pi/4$ was applied in F2. Data was converted to magnitude mode in F2 prior to analysis. ROESY spectra[8,9] with an effective field of γB1 = 8333 Hz and an spin lock time of 200 ms were recorded for a data matrix of 512 x 2048 points covering 8417.5 x 8417.5 Hz. 8 scans were recorded for each increment. Data was linear predicted to 1024 x 2048 points using 32 coefficients prior to States-TPPI type 2D Fourier transformation and a sine square bell shaped window function shifted by $\pi/2$ in both dimensions was applied. For MLEV-17 based TOCSY spectra[10] a data matrix of 512 x 2048 points covering 8417.5 x 8417.5 Hz 2 scans were recorded for each increment. Data was linear predicted to 1024 x 2048 points using 32 coefficients and zero filled to 1024 x 2048 complex points prior to TPPI type 2D Fourier transformation. A cosine square bell shaped window function was applied in both dimensions. For determination of $^{n}J_{HC}$ couplings constants J-HMBC spectra[11] were acquired. A folded data matrix of 1024 x 4096 points covering 21128.5 x 6602.1 Hz was recorded using 16 scans for each increment. A coupling evolution delay of 436.8 ms with a scaling factor of 18 was used. Data was linear predicted to 2048 x 4096 points using 32 coefficients and zero-filled to 2048 x 4096 complex points prior to echo-anti echo type 2D Fourier transformation. A cosine square shaped window function was applied in F1 and a sine shaped window function shifted by $\pi/4$ was applied in F2. Data was converted to magnitude mode in F2 prior to analysis. For determination of coupling constants relevant 1D traces along F1 were extracted using Topspin 3.2 (Bruker Biospin). All spectra were referenced according to the internal solvent signal (^{1}H: $CDCl_3$ = 7.26 ppm and ^{13}C: $CDCl_3$ = 77.16 ppm).[12]

Resonance assignment

1D and 2D spectra were imported into the NMR workbook of ACD Spectrus 2014 for resonance assignment. 1D, HSQC and TOCSY were analyzed to assign protons and carbons of individual amino acid spin systems. Sequential connectivity assignments were achieved using 2D-NOESY experiments.

Additional Tables

Table S1: NOE upper distance bounds of CsA in chloroform measured in this study.

Index	Residue 1	Residue 2	Upper bound [nm]
1	1 HA	6 HA	0.415
2	1 HA	7 HN	0.462
3	7 HN	11 HCN	0.416
4	8 HN	11 HCN	0.435
5	6 HA	11 HCN	0.393
6	8 HA	11 HCN	0.461
7	2 HN	5 HN	0.465
8	1 HA	6 HD	0.463
9	1 HA	7 HB	0.550
10	1 HD1	6 HA	0.413
11	2 HN	5 HB	0.479
12	1 HD1	6 HD	0.499
13	2 HB	5 HB	0.416
14	3 HA	5 HN	0.438
15	1 HG1	3 HCN	0.514
16	8 HN	6 HB	0.519
17	11 HG2	9 HA	0.483
18	8 HN	6 HG	0.449
19	8 HN	6 HD2	0.523
20	1 HCN	10 HD2	0.383
21	11 HA	1 HCN	0.391
22	4 HA	5 HN	0.439
23	1 HA	2 HN	0.354
24	3 HA	4 HCN	0.382
25	7 HA	8 HN	0.428
26	3 HCN	3 HA	0.351
27	8 HN	7 HN	0.462
28	7 HN	6 HA	0.350
29	8 HA	9 HCN	0.384
30	5 HA	6 HCN	0.336
31	2 HA	3 HCN	0.350
32	2 HA	3 HCN	0.364
33	1 HG1	1 HCN	0.420
34	1 HD1	1 HA	0.392
35	1 HH	1 HA	0.374
36	9 HA	8 HB	0.420
37	9 HCN	8 HB	0.372
38	8 HB	8 HN	0.416

Continued on next page

Index	Residue 1	Residue 2	Upper bound [nm]
39	1 HH	2 HN	0.448
40	1 HH	2 HA	0.399
41	10 HG	9 HA	0.438
42	4 HCN	4 HG	0.393
43	10 HD2	9 HA	0.387
44	10 HA	10 HD2	0.390
45	11 HCN	10 HD2	0.428
46	11 HA	10 HD2	0.467
47	9 HD1	8 HN	0.541
48	5 HA	5 HG1	0.397
49	4 HD2	5 HN	0.550
50	5 HN	5 HG1	0.550
51	11 HG2	11 HCN	0.340
52	6 HA	6 HD2	0.395
53	5 HN	5 HG2	0.433
54	7 HB	7 HN	0.392
55	1 HG1	2 HN	0.427
56	4 HCN	5 HB	0.376
57	5 HN	5 HB	0.394
58	9 HA	9 HD1	0.499
59	1 HG	1 HA	0.410
60	11 HB	11 HCN	0.388
61	4 HCN	4 HD1	0.422
62	6 HCN	6 HB	0.378
63	6 HCN	6 HG	0.471
64	6 HCN	6 HB	0.404
65	1 HG	1 HCN	0.384
66	5 HB	6 HCN	0.377
67	1 HD2	1 HA	0.432
68	4 HCN	4 HB	0.362
69	1 HG1	1 HD2	0.529
70	1 HG	1 HZ	0.394
71	1 HG1	1 HZ	0.468
72	1 HD1	1 HE	0.446
73	1 HB	1 HZ	0.443
74	1 HH	1 HE	0.354
75	10 HG	9 HB	0.429
76	4 HB	4 HD1	0.416
77	1 HG1	2 HG	0.396
78	1 HH	2 HG	0.440
79	11 HG2	10 HG	0.336
80	1 HD1	1 HZ	0.418
81	1 HG1	1 HD1	0.419

Continued on next page

Index	Residue 1	Residue 2	Upper bound [nm]
82	4 HB	4 HD1	0.416
83	1 HG	1 HD2	0.262

Table S2: Temperature coefficient for amide groups of CsA in chloroform measured in this study.

Index	Residue	Temperature coefficient [ppb/K]
1	Abu-2	-2.5
2	Val-5	-1.2
3	Ala-7	-5.5
4	D-Ala-8	-0.8

Table S3: ^3J coupling constants of CsA in chloroform measured in this study. The Karplus relationship is of the form $^3J(\phi) = A \cdot cos^2(\phi) + B \cdot cos(\phi) + C$. Parameters were estimated following the Bayesian procedure described in Ref. 13.

Index	Residue 1	Residue 2	Coupling [Hz]	Karplus parameters		
				A	B	C
1	2 HN	2 HA	9.70	7.13	-1.31	1.56
2	5 HN	5 HA	8.35	7.13	-1.31	1.56
3	7 HN	7 HA	7.45	7.13	-1.31	1.56
4	8 HN	8 HA	7.90	7.13	-1.31	1.56

Table S4: NOE upper distance bounds of CsA in chloroform from 1985.[14]

Index	Residue 1	Residue 2	Upper bound [nm]
1	1 HA	6 HA	0.350
2	1 HA	7 HN	0.350
3	7 HN	11 HCN	0.350
4	8 HN	11 HCN	0.350
5	8 HA	11 HCN	0.350
6	1 HB	6 HA	0.300
7	1 HA	2 HN	0.300
8	2 HA	3 HCN	0.350
9	3 HA	4 HCN	0.250
10	4 HA	5 HN	0.300
11	4 HCN	5 HN	0.300
12	5 HN	5 HA	0.300
13	5 HA	6 HCN	0.200
14	7 HA	7 HN	0.350
15	7 HN	8 HN	0.350
16	8 HN	8 HA	0.350
17	8 HA	9 HCN	0.200
18	9 HA	10 HA	0.250
19	10 HA	11 HCN	0.300
20	11 HCN	11 HA	0.350
21	11 HA	1 HCN	0.250
22	1 HB	1 HCN	0.350
23	1 HB	1 HA	0.300
24	1 HA	1 HD1	0.350
25	4 HCN	4 HB	0.300
26	4 HCN	4 HG	0.350
27	4 HA	4 HD1	0.350
28	4 HA	4 HB	0.300
29	4 HCN	5 HG1	0.300
30	5 HG1	5 HA	0.350
31	5 HA	5 HB	0.300
32	5 HG1	6 HCN	0.300
33	6 HCN	6 HB	0.350
34	6 HA	6 HB	0.350
35	6 HA	6 HD1	0.350
36	7 HN	7 HB	0.300
37	7 HA	7 HB	0.250
38	8 HN	8 HB	0.300
39	8 HA	8 HB	0.250
40	8 HB	9 HCN	0.350
41	9 HCN	9 HB	0.300

Continued on next page

Index	Residue 1	Residue 2	Upper bound [nm]
42	9 HB	9 HA	0.350
43	9 HA	10 HD1	0.350
44	9 HA	9 HG	0.350
45	10 HCN	10 HB	0.250
46	11 HCN	11 HB	0.250
47	11 HCN	11 HG1	0.250
48	11 HG1	1 HCN	0.300
49	11 HCN	11 HB	0.250
50	9 HB	9 HG	0.350
51	9 HD1	10 HD1	0.350

Table S5: NOE upper distance bounds of CsA in chloroform from 1990.[15]

Index	Residue 1	Residue 2	Upper bound [nm]
1	1 HA	6 HA	0.269
2	1 HA	7 HN	0.300
3	7 HN	11 HCN	0.394
4	8 HN	11 HCN	0.400
5	8 HA	11 HCN	0.399
6	2 HN	5 HN	0.321
7	2 HN	6 HA	0.357
8	1 HA	6 HD1	0.460
9	1 HA	7 HB	0.517
10	1 HB	6 HA	0.432
11	1 HB	7 HN	0.472
12	1 HD1	6 HA	0.397
13	1 HD2	6 HA	0.351
14	2 HN	5 HB	0.319
15	2 HB	5 HB	0.298
16	1 HA	3 HCN	0.527
17	3 HCN	5 HN	0.411
18	3 HA	5 HN	0.336
19	5 HN	3 HA	0.366
20	6 HA	8 HN	0.357
21	9 HA	11 HCN	0.459
22	1 HB	3 HCN	0.283
23	1 HB	5 HN	0.369
24	1 HD1	3 HCN	0.550
25	2 HN	11 HG1	0.470
26	5 HG1	7 HA	0.427
27	6 HG	8 HN	0.275
28	6 HD1	8 HN	0.477
29	1 HCN	1 HA	0.432
30	1 HCN	2 HN	0.479
31	1 HCN	11 HA	0.301
32	1 HA	2 HN	0.221
33	1 HA	11 HCN	0.519
34	2 HN	2 HA	0.311
35	2 HN	3 HCN	0.450
36	2 HA	3 HCN	0.318
37	3 HCN	3 HA	0.356
38	3 HA	4 HCN	0.283
39	4 HCN	4 HA	0.437
40	4 HA	5 HN	0.297
41	5 HN	5 HA	0.296

Continued on next page

Index	Residue 1	Residue 2	Upper bound [nm]
42	5 HN	4 HCN	0.349
43	6 HA	7 HN	0.213
44	7 HN	7 HA	0.297
45	7 HN	8 HN	0.284
46	7 HA	8 HN	0.292
47	8 HN	8 HA	0.284
48	8 HN	9 HCN	0.569
49	8 HA	9 HCN	0.283
50	9 HCN	9 HA	0.471
51	9 HA	10 HA	0.180
52	10 HA	11 HCN	0.318
53	1 HCN	1 HD2	0.415
54	1 HCN	1 HD1	0.572
55	1 HCN	11 HB	0.441
56	1 HCN	11 HG1	0.574
57	1 HA	1 HB	0.233
58	1 HA	1 HD1	0.372
59	1 HA	1 HD2	0.311
60	1 HB	2 HN	0.274
61	1 HD1	2 HN	0.527
62	1 HD2	2 HN	0.523
63	2 HN	2 HB	0.315
64	2 HA	2 HB	0.285
65	4 HCN	4 HB	0.336
66	4 HCN	5 HG1	0.421
67	4 HA	4 HB	0.249
68	4 HA	4 HG	0.315
69	4 HA	4 HD1	0.354
70	5 HN	5 HB	0.249
71	5 HN	5 HG1	0.454
72	5 HA	5 HB	0.318
73	5 HA	5 HG1	0.383
74	5 HB	6 HCN	0.410
75	5 HG1	6 HCN	0.447
76	6 HCN	6 HB	0.340
77	6 HA	6 HB	0.301
78	6 HA	6 HG	0.327
79	6 HA	6 HD1	0.395
80	6 HG	7 HN	0.401
81	6 HD1	7 HN	0.445
82	7 HN	7 HB	0.358
83	7 HA	8 HB	0.470
84	7 HB	8 HN	0.443

Continued on next page

Index	Residue 1	Residue 2	Upper bound [nm]
85	8 HN	8 HB	0.344
86	9 HCN	8 HB	0.521
87	9 HCN	9 HB	0.347
88	9 HA	9 HB	0.293
89	9 HA	9 HG	0.281
90	9 HA	9 HD1	0.390
91	9 HA	10 HB	0.361
92	9 HA	10 HG	0.294
93	9 HB	10 HA	0.384
94	10 HCN	10 HB	0.395
95	10 HA	10 HB	0.282
96	10 HA	10 HG	0.308
97	11 HCN	11 HB	0.310
98	11 HA	11 HB	0.297
99	1 HB	1 HD1	0.387
100	1 HB	1 HD2	0.320
101	1 HD1	1 HD2	0.459
102	6 HB	6 HG	0.271
103	6 HB	6 HD1	0.411
104	9 HB	10 HG	0.267

Table S6: Average backbone atom-positional RMSD between the crystal structures CRYSTC (DEKSAN[14]) and CRYSTO (2Z6W[16]) and the metastable sets in chloroform (C1, C2 and C3) and in water (W1, W2, W3, W4 and W5). The smallest RMSD value in each column is marked in bold font.

Chloroform			**Water**		
Metastable set	CRYSTO	CRYSTC	Metastable set	CRYSTO	CRYSTC
C1	0.225	**0.122**	W1	0.197	0.338
C2	0.209	0.342	W2	0.187	0.255
C3	**0.166**	0.232	W3	**0.117**	0.260
			W4	0.218	**0.084**
			W5	0.167	0.226

Additional Figures

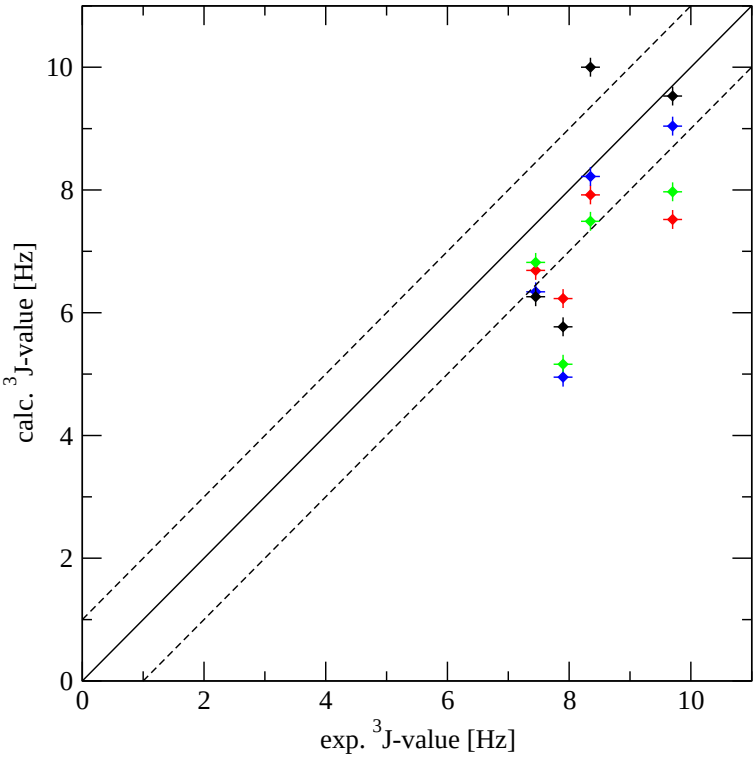

Figure S1: Comparison of the experimental and calculated $^3J(\mathrm{H}_N\text{-}\mathrm{H}_{C_\alpha})$-coupling constants for CRYSTC (black), the total 10 μs in chloroform (green), and the metastable sets C1 (red) and C2 (blue). The experimental values are listed in Table S3.

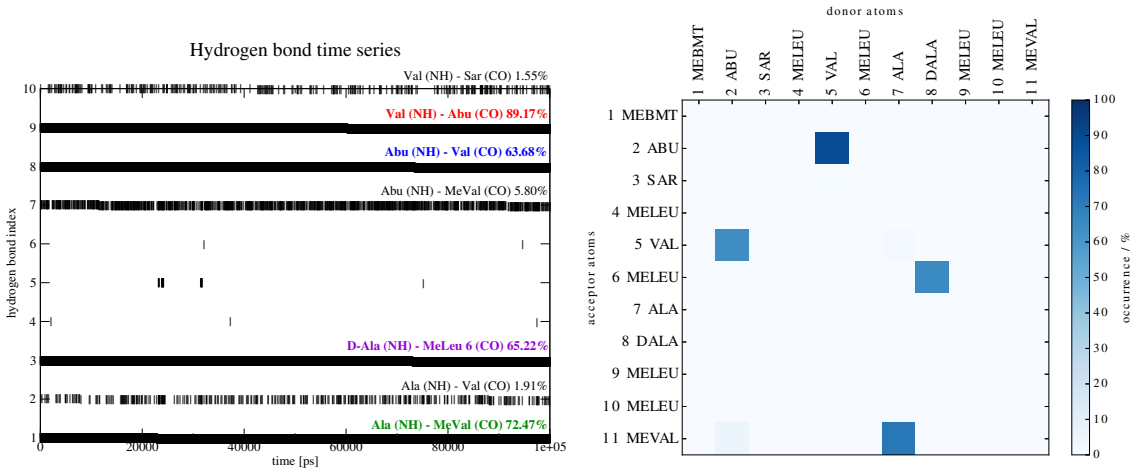

Figure S2: Time series of the H-bonds occurring in more than 1% of the trajectory (left), occurrence of H-bonds in percentage (middle), and time series of the distances between atoms forming the backbone H-bonds (right) for the simulation at 300 K in chloroform starting from CRYSTC.

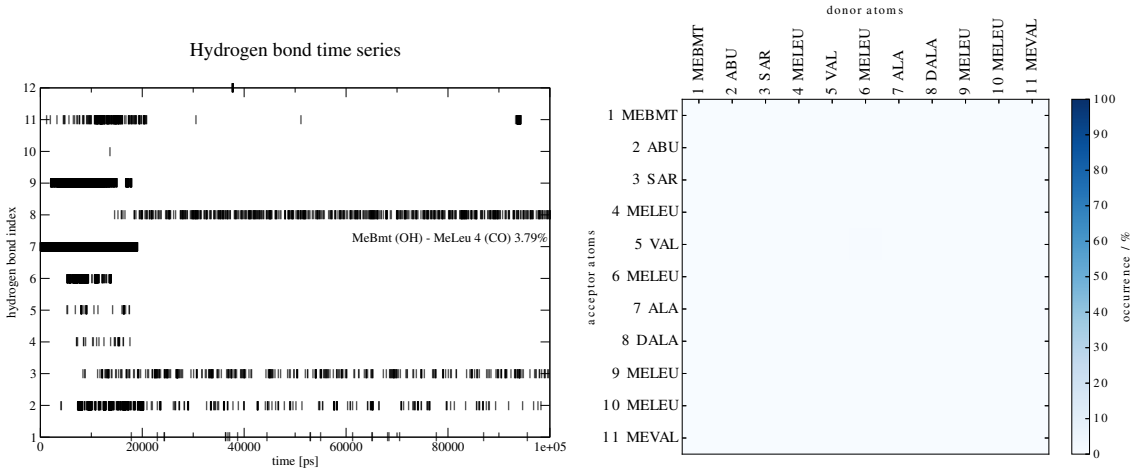

Figure S3: Time series of the H-bonds occurring in more than 1% of the trajectory (left), occurrence of H-bonds in percentage (middle), and time series of the distances between atoms forming the backbone H-bonds (right) for the simulation at 300 K in water starting from CRYSTO.

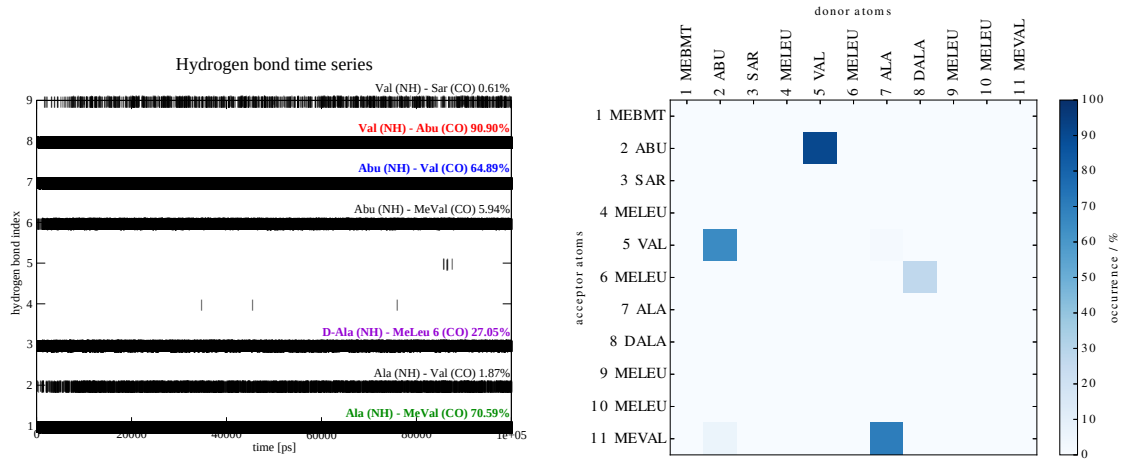

Figure S4: Time series of the H-bonds occurring in more than 1% of the trajectory (left), occurrence of H-bonds in percentage (middle), and time series of the distances between atoms forming the backbone H-bonds (right) for the simulation at 300 K in water starting from CRYSTC.

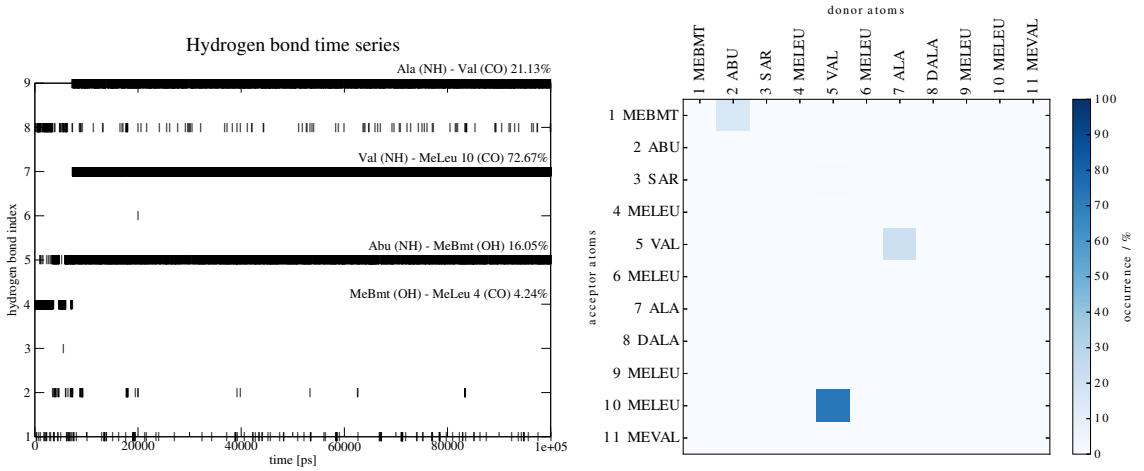

Figure S5: Time series of the H-bonds occurring in more than 1% of the trajectory (left), occurrence of H-bonds in percentage (middle), and time series of the distances between atoms forming the backbone H-bonds (right) for the simulation at 300 K in chloroform starting from CRYSTO.

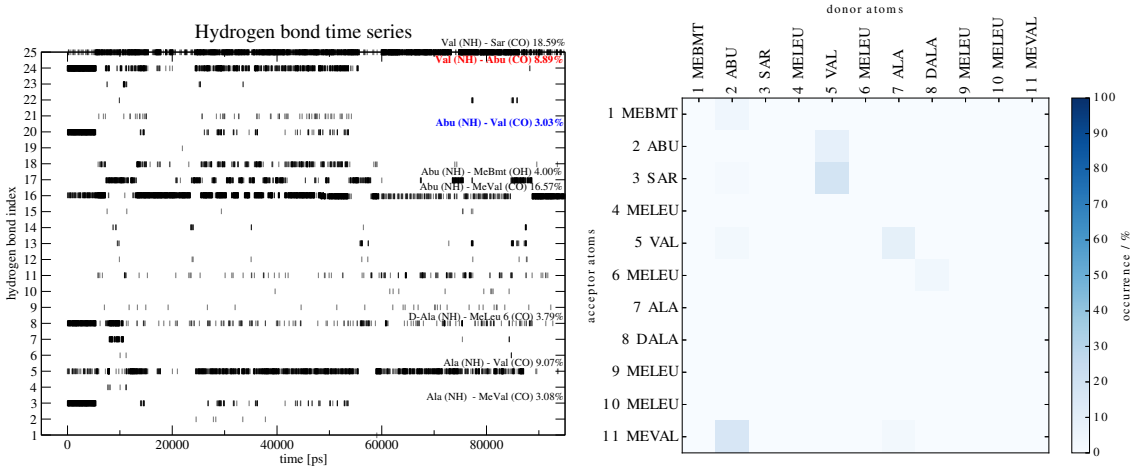

Figure S6: Time series of the H-bonds occurring in more than 1% of the trajectory (left), occurrence of H-bonds in percentage (middle), and time series of the distances between atoms forming the backbone H-bonds (right) for the simulation at 400 K in water starting from CRYSTC.

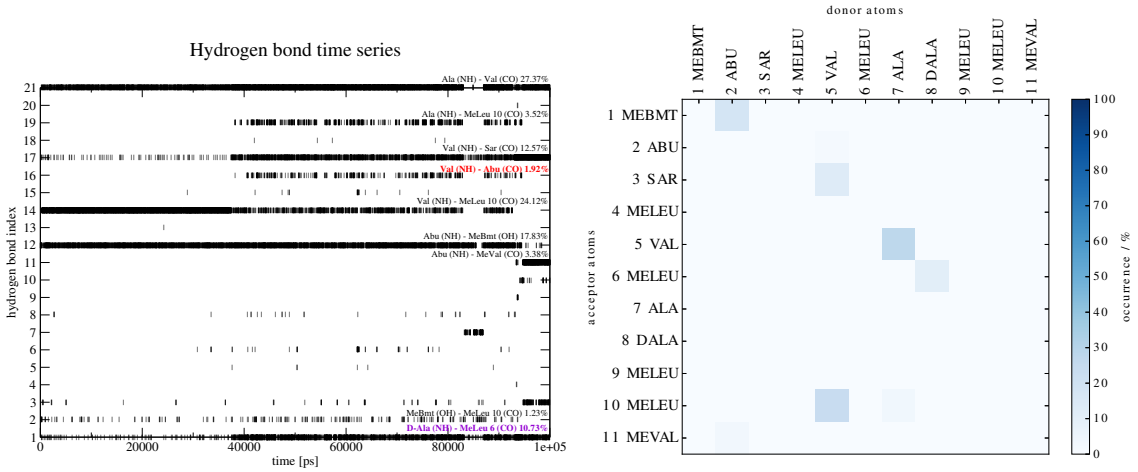

Figure S7: Time series of the H-bonds occurring in more than 1% of the trajectory (left), occurrence of H-bonds in percentage (middle), and time series of the distances between atoms forming the backbone H-bonds (right) for the simulation at 400 K in chloroform starting from CRYSTO.

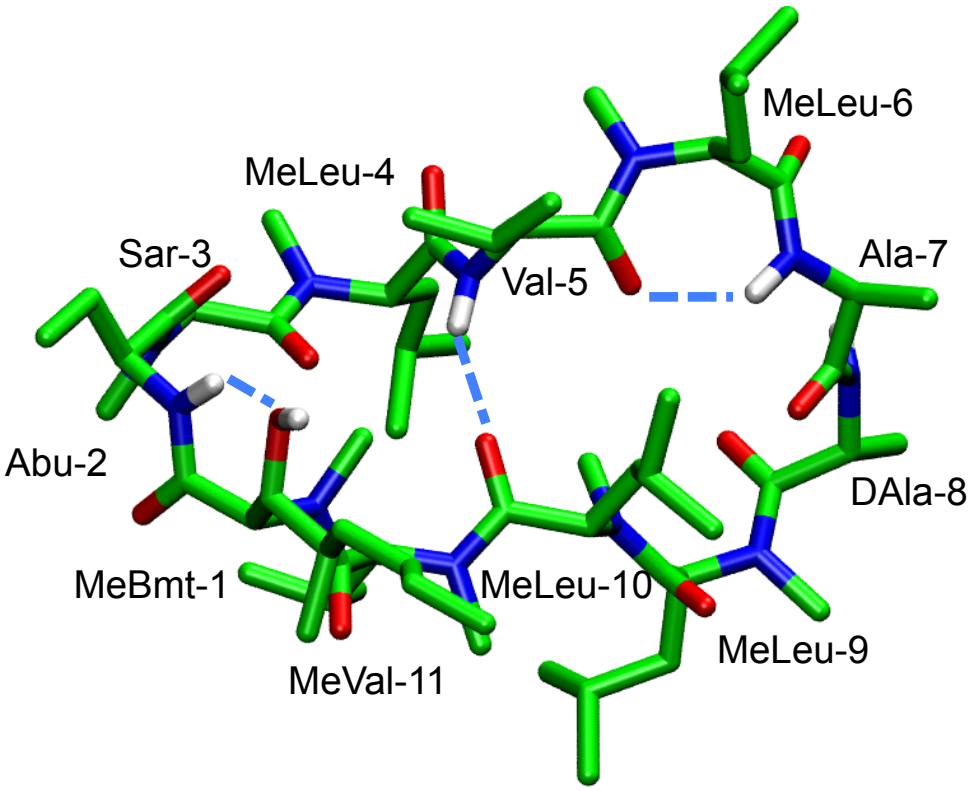

Figure S8: Snapshot at 99.45 ns from the simulation at 300 K in chloroform starting from CRYSTO. H-bonds are marked with dashed light blue lines. Figure was generated with VMD.[17]

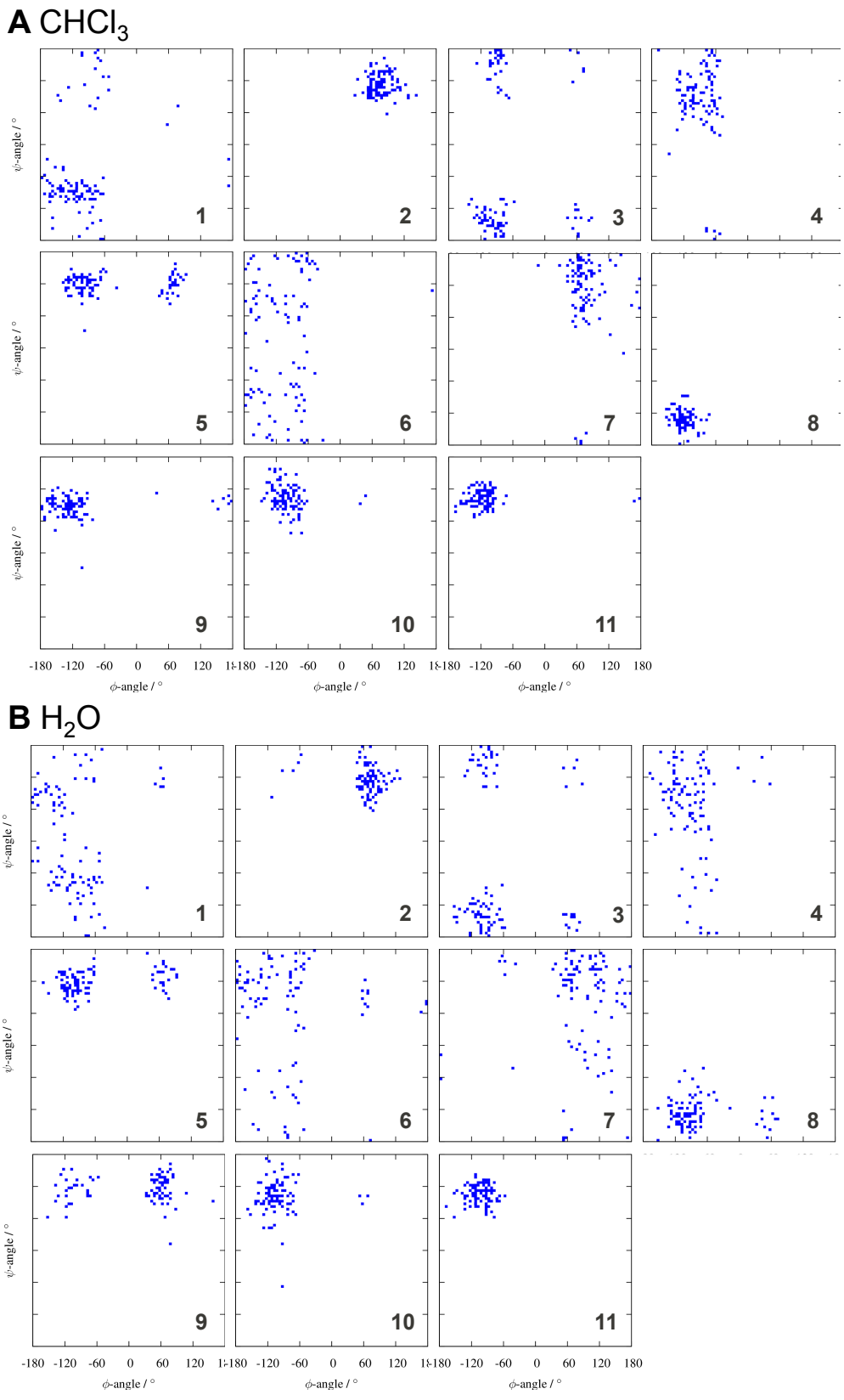

Figure S9: Ramachandran plots of the backbone dihedral angles for the 100 seed conformations in chloroform (A) and in water (B).

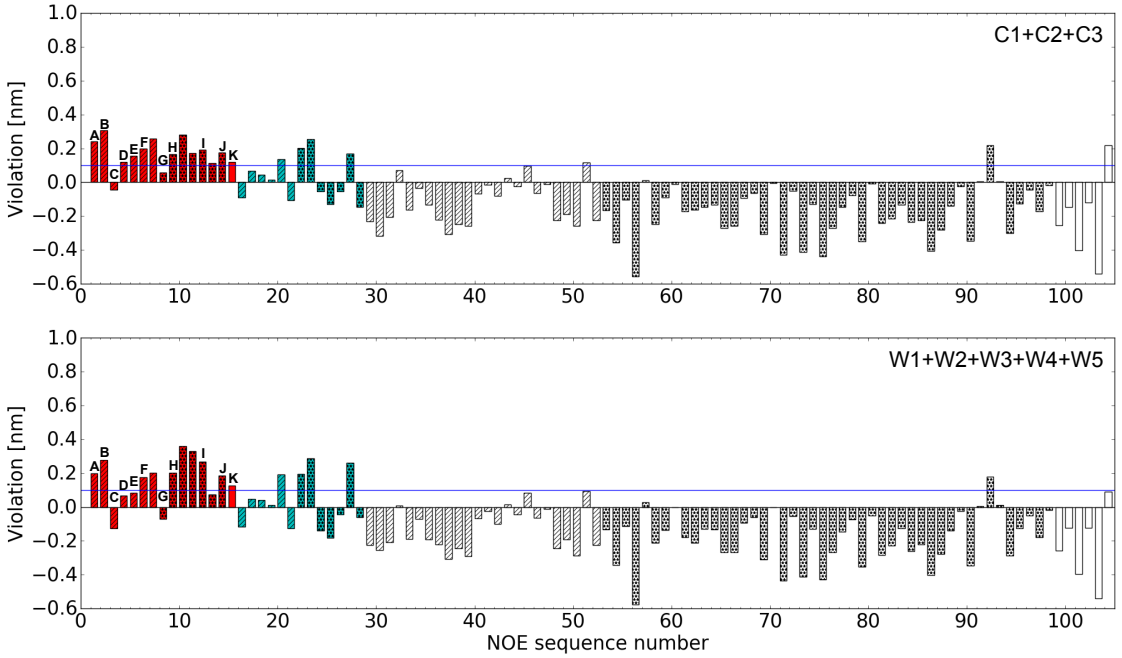

Figure S10: Violations of the experimental NOE upper distance bounds from the 1990 set[15] as a function of the NOE sequence number. The NOE distances are grouped into "intercycle" (red), "intermediate" (cyan) and NOE distances from neighboring or the same residues (white), as well as labeled based on the nature of the protons: backbone–backbone (stripes), backbone–side chain (stars) and side chain–side chain (plain). Hydrogen pairs corresponding in both sets are marked with capital letters according to labels in the first column of Table 4. Top: MSM in chloroform with the metastable sets C1, C2 and C3. Bottom: MSM in water with the metastable sets W1, W2, W3, W4 and W5.

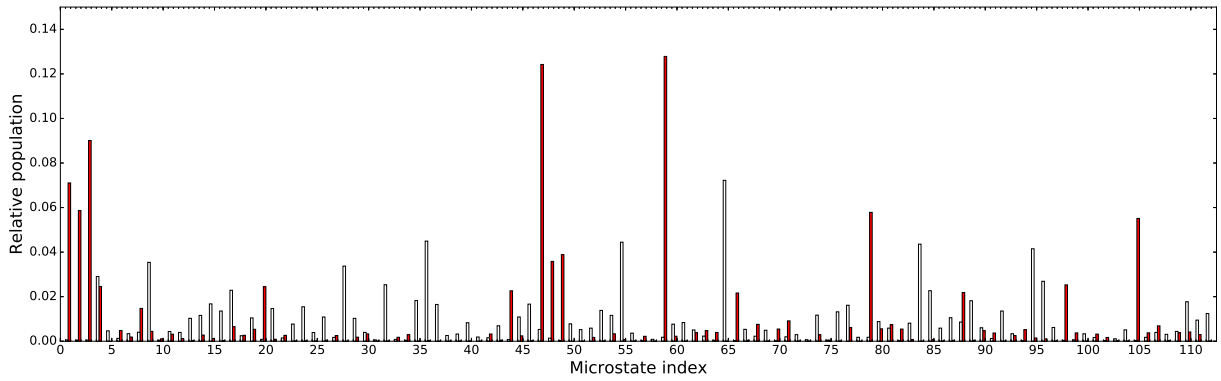

Figure S11: Relative populations of the microstates in chloroform (red) and water (white).

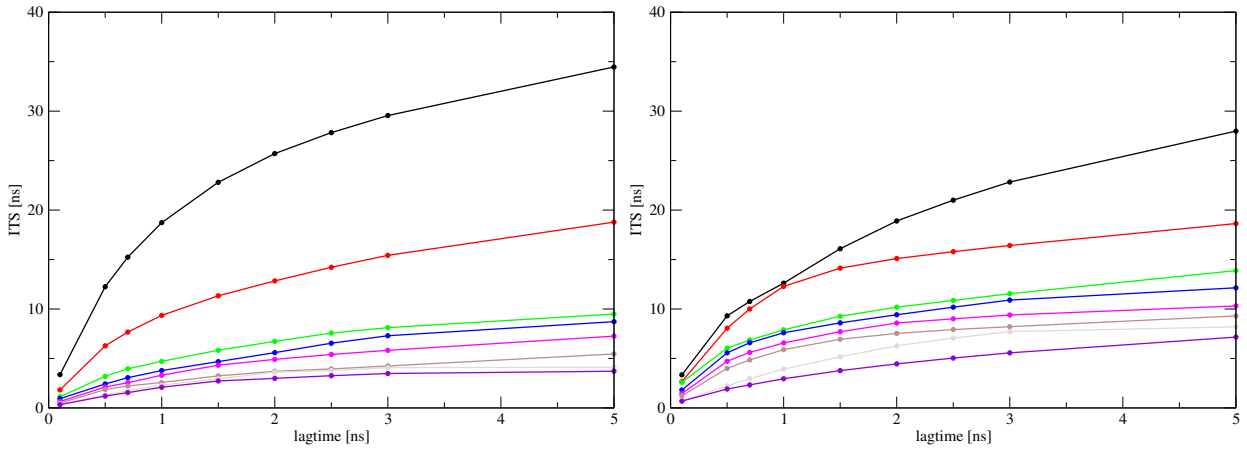

Figure S12: Implied timescales for interconversion processes described by MSMs in chloroform (left) and in water (right).

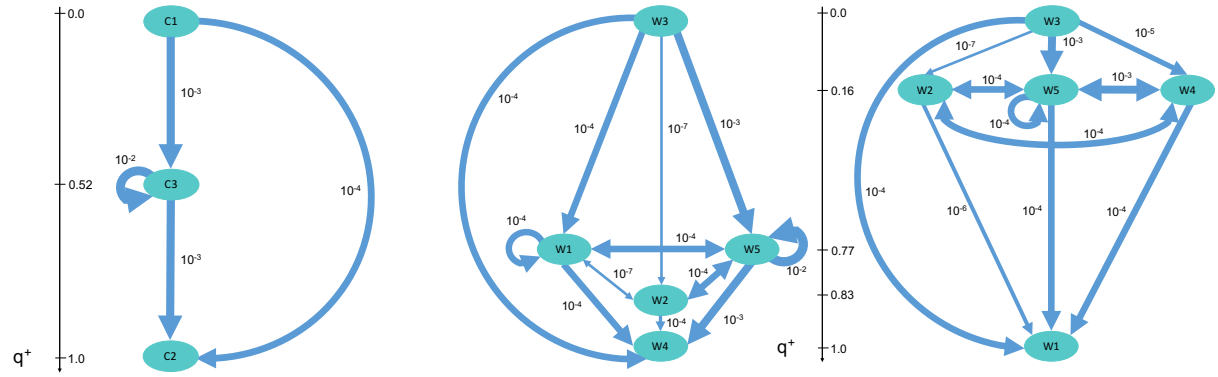

Figure S13: Flux between selected metastable sets in chloroform (left) and in water (right). The y-axis displays the forward committor probabilities, the thickness of the arrow indicates the net flux between each pair of metastable set.

References

(1) Vonkienlin, M.; Moonen, C. T. W.; Vandertoorn, A.; Vanzijl, P. C. M. Rapid Recording of Solvent-Suppressed 2D COSY Spectra with Inherent Quadrature Detection Using Pulsed Field Gradients. *J. Magn. Reson.* **1991**, *93*, 423–429.

(2) Carpenter, T. A.; Colebrook, L. D.; Hall, L. D.; K.Pierens, G. Applications of Gradient-Selective COSY and DQCOSY to Brucine and Gibberellic-Acid. *Magn. Reson. Chem.* **1992**, *30*, 768–773.

(3) Kay, L. E.; Keifer, P.; Saarinen, T. Pure Absorption Gradient Enhanced Heteronuclear Single Quantum Correlation Spectroscopy with Improved Sensitivity. *J. Am. Chem. Soc.* **1992**, *114*, 10663–10665.

(4) Lindorff-Larsen, K.; Piana, S.; Palmo, K.; Maragakis, P.; Klepeis, J. L.; Dror, R. O.; Shaw, D. E. Improved Side-Chain Torsion Potentials for the Amber ff99SB Protein Force Field. *Proteins* **2010**, *78*, 1950–1958.

(5) Kupce, E. Applications of Adiabatic Pulses in Biomolecular Nuclear Magnetic Resonance. *Method. Enzymol.* **2001**, *338*, 82–111.

(6) Bax, A.; Summers, M. F. H-1 and C-13 Assignments from Sensitivity-Enhanced Detection of Heteronuclear Multiple-Bond Connectivity by 2D Multiple Quantum NMR. *J. Am. Chem. Soc.* **1986**, *108*, 2093–2094.

(7) Meissner, A.; Sorensen, O. W. Economizing Spectrometer Time and Broadband Excitation in Small-Molecule Heteronuclear NMR Correlation Spectroscopy. Broadband HMBC. *Magn. Reson. Chem.* **2000**, *38*, 981–984.

(8) Bax, A.; Davis, D. G. Practical Aspects of Two-Dimensional Transverse NOE Spectroscopy. *J. Magn. Reson.* **1985**, *63*, 207–213.

(9) Hwang, T. L.; Shaka, A. J. Cross Relaxation without TOCSY - Transverse Rotating-Frame Overhauser Effect Spectroscopy. *J. Am. Chem. Soc.* **1992**, *114*, 3157–3159.

(10) Bax, A.; Davis, D. G. MLEV-17-Based Two-Dimensional Homonuclear Magnetization Transfer Spectroscopy. *J. Magn. Reson.* **1985**, *65*, 355–360.

(11) Meissner, A.; Sorensen, O. W. Measurement of J(H,H) and Long-Range J(X,H) Coupling Constants in Small Molecules. Broadband XLOC and J-HMBC. *Magn. Reson. Chem.* **2001**, *39*, 49–52.

(12) Gottlieb, H. E.; Kotlyar, V.; Nudelman, A. NMR Chemical Shifts of Common Laboratory Solvents as Trace Impurities. *J. Org. Chem.* **1997**, *62*, 7512–7515.

(13) Habeck, M.; Rieping, W.; Nilges, M. Bayesian Estimation of Karplus Parameters and Torsion Angles from Three-Bond Scalar Couplings Constants. *J. Magn. Reson.* **2005**, *177*, 160–165.

(14) Loosli, H.-R.; Kessler, H.; Oschkinat, H.; Weber, H.-P.; Petcher, T. J.; Widmer, A. Peptide Conformations. Part 31. The Conformation of Cyclosporin A in the Crystal and in Solution. *Helv. Chim. Acta* **1985**, *68*, 682–704.

(15) Kessler, H.; Kock, M.; Wein, T.; Gehrke, M. Reinvestigation of the Conformation of Cyclosporin A in Chloroform. *Helv. Chim. Acta* **1990**, *73*, 1818–1831.

(16) Kajitani, K.; Fujihashi, M.; Kobayashi, Y.; Shimizu, S.; Tsujimoto, Y.; Miki, K. Crystal Structure of Human Cyclophilin D in Complex with Cyclosporin A. *Proteins* **2008**, *7*, 1635–1639.

(17) Humphrey, W.; Dalke, A.; Schulten, K. VMD - Visual Molecular Dynamics. *J. Mol. Graph.* **1996**, *14*, 33–38.